Heliyon 10 (2024) e38290

Contents lists available at ScienceDirect

Heliyon

journal homepage: www.cell.com/heliyon

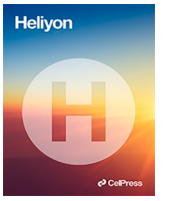

Research article

Effect of magnetic anisotropy and interaction on spatial focused hyperthermia for rotating and oscillating fields

Vilmos Vékony [a,b,c,*], István G. Márián [b,c], István A. Szabó [b]

[a] University of Debrecen, Doctoral School of Physics, 4032, Debrecen, Egyetem Tér 1, Hungary
[b] Department of Solid State Physics, Faculty of Science and Technology, University of Debrecen, H-4039, Debrecen, Bem tér 18/b, Hungary
[c] HUN-REN Institute for Nuclear Research, Bem tér 18/c, Debrecen, P.O. Box 51, H-4001, Hungary

ARTICLE INFO

Keywords:
Magnetic nanoparticle
Hyperthermia
Diffusion jump model
Interacting system

ABSTRACT

The behavior of magnetic nanoparticles in a time-varying magnetic field has several practical applications. One of these is hyperthermia used in the treatment of cancer. The nanoparticles injected in the tumor cells release the energy absorbed from the time dependent external magnetic field in the form of heat to its environment in a well-localized way. The aim of the research in this area is to maximize the amount of the dissipated energy. Using a combination of an oscillating and static magnetic field, this dissipated energy can be more focused in space. In this article, we investigated whether this spatial focusing is also present using a rotating and static field together. Furthermore, we investigated the effects of anisotropy and interaction between nanoparticles on this spatial focusing effect using the jump-diffusion model for Néel relaxation in both cases. This kinetic Monte Carlo (MC) method was validated and compared with the stochastic Landau-Lifshitz-Gilbert (SLLG) equation based model. We have shown that the spatial focusing effect is also present for these non-idealized experimentally realizable cases. Also, the effect of rotating magnetic field on magnetic nanoparticles was not investigated in kinetic Monte Carlo simulations before.

1. Introduction

Hyperthermia is a complementary procedure to other conventional tumor treatment methods. By placing ferromagnetic nanoparticles in an alternating external field, their magnetization vector changes and the nanoparticle will relax through a frictional process. As a result of the dissipation, the temperature of tumor cells containing nanoparticles increases and they die. Therefore, the method is suitable for the treatment of cancer [1–9].

Hyperthermic research focuses on maximizing heat loss. Hyperthermic treatments have several advantages over traditional tumor treatment methods. The magnetic nanoparticles can be well positioned with the external magnetic field, so they actually exert their effect only where they are needed, unlike with other procedures, where the surrounding tissues can also be severely damaged. The resulting side effects are negligible, compared to chemotherapy, where, due to the non-selective burden on the body, "poisoning symptoms", e.g. vomiting, headache, and fever may also occur. Hyperthermia is also suitable for treating types of tumors that are difficult to access surgically, such as brain tumors [10]. In this case, the blood-brain barrier prevents the delivery of drug molecules to tumor cells. However, cancer cells in the brain are sensitive to heat treatment.

* Corresponding author. HUN-REN Institute for Nuclear Research, Bem tér 18/c, Debrecen, P.O. Box 51, H-4001, Hungary
E-mail address: vekony.vilmos@atomki.hu (V. Vékony).

https://doi.org/10.1016/j.heliyon.2024.e38290
Received 28 May 2024; Received in revised form 20 September 2024; Accepted 20 September 2024
Available online 22 September 2024

Two types of approximations are used for the temporal change of the magnetization vector. One is the "rigid dipole" and the other is the "fixed nanoparticle" [11,12]. In the former case, the magnetization vector is rigidly attached to the crystal and the nanoparticle can rotate. In the other case, the nanoparticle cannot move, only the internal change of the magnetization vector is possible. So, the changing process of magnetization vector can take place by mechanical rotation and/or by internal friction. The former is the Brown relaxation, the latter is called the Néel relaxation. From the point of view of tumor therapy, the latter is more important, since the nanoparticles cannot mechanically move once they are injected into the tumor cells. Therefore, it is not necessary to consider the mechanical rotation during the simulations. On the other hand, the anisotropy of the material and the strength of the dipole-dipole interaction are of greater importance for the loss.

Utilizing the rise in body temperature for medical purposes has a long-standing historical background. Nonetheless, employing whole-body hyperthermia presents challenges due to the arduous task of raising the core temperature, which can result in significant disadvantages. Therefore, focusing on localized heating becomes crucial. The more targeted the hyperthermia treatment, the greater its effectiveness. Several studies prove that the practical application of local hyperthermia is of great importance [13–17]. The amplitude and frequency of the excitation field cannot be arbitrary. As a result of a time-varying magnetic field, eddy currents can be generated in the human body. This results in an unwanted heating effect, which can even damage healthy tissues. An upper limit was defined for the product of the two quantities (Hergt-Dutz limit): $Hf \leq 5{*}10^8\ A/(ms)$ [18]. The frequency and field strength range used during the procedure is 0.05–1.2 MHz and 0–15 kA/m, respectively [19–21]. The most commonly used magnetic nanoparticle (MNP) materials are the iron oxide nanoparticles [22–24].

There are several models for describing the temporal change of the magnetization vector. Among these, the stochastic Landau-Lifshitz-Gilbert equation is the most frequently used. We use another frequently used model in this work, which is based on the kinetic Monte Carlo method. This treats the reversal of the magnetization vector between two stable states as a diffusion jump [25]. The advantage of this model over the model based on the SLLG equation is that the same process can be run with much less CPU time. In this way, more complex systems (taking into account dipole-dipole interaction between MNPs) can also be simulated. Furthermore, the damping parameter used in the SLLG model is an arbitrarily defined parameter. Little research deals with the experimental determination of this quantity for different materials. In contrast, kinetic Monte Carlo model results have often been compared with experimental results in relatively good matches in the literature. In addition, it is always useful to investigate interesting effects with more than one model to increase the confidence in new theoretical results like the spatial focusing effect mentioned below [50,58].

Several researches are currently investigating the effect of the dipole-dipole interaction on energy loss. Typically, the presence of dipole-dipole interaction reduces the energy loss [26–32]. But in the literature [33] found that if the clusters of densely-packed nanoparticles are small enough (it contains few nanoparticles), then the heating efficiency is higher, than at the non-interacting particles. The reason for this is the shape anisotropy of these small clusters. If the size of these clusters are increasing, then the shape of the clusters become more isotropic and therefore the dissipated energy is decreasing.

Besides that, in these and most hyperthermic investigations as well an oscillating magnetic field is examined. Relatively few articles deal with magnetic nanoparticles placed in a rotating field and with the energy loss resulting from the process, but the number of these articles are increasing [34,35]. It was found that rotating magnetic field could be useful at the local heat generation of the malignant cells. Other medical uses of the rotating magnetic field are also mentioned in the literature. For example, rotating magnetic field can be used for protein detection [36]. It has been reported in the literature that using rotating magnetic field and static magnetic field perpendicular to the plane of rotation can be used to more easily deliver magnetic nanoparticles through porous materials (enhanced diffusion) than using static fields alone [37].

In the literature, both theoretical and experimental investigations have been carried out for the case where an oscillating magnetic field was applied with a static magnetic field parallel or perpendicular to the oscillation [38–46]. The results obtained show that in both cases, the energy loss decreases with increasing the static field. In practice, if a gradient magnetic field is applied with an oscillating magnetic field, the method may be suitable for a more accurate spatial focusing of the energy loss. However, the combination of a rotating magnetic field and a static magnetic field parallel or perpendicular to the plane of rotation has rarely been addressed in the literature. In a previous article, we examined the effect of the application of an extra static field on the energy loss of non-interacting, isotropic magnetic nanoparticles in an oscillating and rotating magnetic field. In the case of rotating field there is a maximum if the magnitude of static field is equal to the amplitude and the static field placed in the plane of the rotating field. In the case of oscillating and perpendicular static field the maxima appeared at zero static field [58].

In the literature, the difference between interacting and noninteracting systems has been investigated for oscillating and static magnetic field parallel to the oscillation [46]. It was obtained that the interaction reduces the energy loss at the peak value. However, in our previous paper we have shown that a static magnetic field perpendicular to the oscillation can achieve better spatial focusing than a parallel magnetic field. It is an open question how this spatial focusing effect is affected (for the rotating case and the oscillating case with the same parameters) by the fact that the nanoparticles have anisotropy, and how the interaction between MNPs affects the energy loss. In this article, we show how the anisotropy will affect the width and location of the peaks, and how much the interaction changes the localization and magnitude of loss.

2. Theoretical method

We used the kinetic Monte Carlo model to describe the time evolution of the magnetization of magnetic nanoparticles. These calculations are based on kinetic Monte Carlo simulations.

In a many-particle interacting system, assuming energy minimums, the magnetization of a nanoparticle can have two equilibrium states: "up" and "down". The magnetization of the nanoparticle is a 3 dimensional vector and the "up" and "down" states for a given

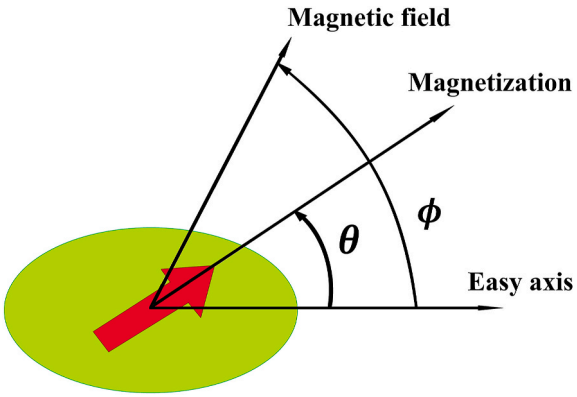

Fig. 1. The angles between the anisotropy axis and the magnetization of a magnetic nanoparticle or the magnetic field.

nanoparticle are relative to the anisotropy axis. More precisely, the projection of the magnetization vector on the uniaxial anisotropy axis can be interpreted as the "up" or "down" states, but the magnetization vector can be in any direction. The energy of a nanoparticle can be obtained as follows:

$$E(\theta,\phi) = KV\sin^2\theta - m\mu_0 H_{tot}\cos(\theta-\phi) \tag{1}$$

where θ is the angle between the magnetization vector and the anisotropy axis, ϕ is the angle between the H_{tot} total magnetic field and the anisotropy axis (Fig. 1.), K is the anisotropy energy density, V is the particle volume, m is the particle magnetic moment, μ_0 is the vacuum permeability. The total magnetic field consists of the applied external magnetic field ($\overline{H}_{ext}$) and the dipole field ($\overline{H}_{dip}$) generated by the particles. The dipole field acting on a given particle and generated by other particles can be defined as follows:

$$\overline{H}_{dip} = \frac{M_s V}{4\pi}\sum_{i\neq j}\frac{3\left(\overline{m}_j\overline{e}_{ij}\right)\overline{e}_{ij} - \overline{m}_j}{r_{ij}^3} \tag{2}$$

where $\overline{m}_j$ is the unit vector in the direction of the magnetization of the jth particle and $\overline{e}_{ij}$ is the unit vector connecting the ith particle to the jth particle. Here we used the open boundary condition.

The time evolution of magnetization is given as follows. The time of a magnetization cycle has been divided into several time steps (t_{step}), where the magnetic field step intervals are approximately constant. This was 2000 step intervals when the program was run. The length of a time step is derived from the periodic time of the oscillating or rotating field, the 2000th part of it. For the time step validation (Fig. 16.), we examined how fine the time step intervals should be to achieve a certain fixed value of energy loss. In one simulation, the program calculated the time variation of the magnetization of 1000 particles. The particles were placed on a 10x10x10 cube lattice. The lattice points are characterized by 3-dimensional vectors with Cartesian coordinates. The lattice constant (the distance between the centers of the particles) was set to a multiple of the particle diameter. After that, we made a small random deviation in the position of the nanoparticles. This sample preparation process happens before the simulation. When we turn on the external magnetic field, the positions of the particles are already fixed. We used this configuration to avoid the clustering effects while we can change the dipole-dipole interaction with a single parameter. The main algorithm is similar to Refs. [48,49]:

1) First, the 3-dimensional spatial location of the nanoparticles, their magnetization, and the direction of their anisotropy axis were given. In most simulations, the nanoparticles were randomly oriented.
2) For each particle, the total magnetic field has been calculated based on the magnitude and direction of the external field and the dipole field generated by the other particles.
3) For each particle, the function $E(\theta)$ is recorded at the given time step over a range of 360°. In most cases, there will be two minima and one maximum of the function (in some cases there is one minimum). These will be the previously mentioned "up" and "down" magnetization states. The angles and energy values corresponding to the minima and maxima are (θ_1, E_1), (θ_2, E_2) and (θ_3, E_3).
4) The nanoparticle will be in one of the two minimum states. The energy difference between the maximum and the minimum will greatly affect the probability of the jump. The jumping frequency between $\theta_1 \rightarrow \theta_2$ states can be defined as follows:

$$\nu_{12} = \nu_0\exp\left(-\frac{E_3 - E_1}{k_B T}\right) \tag{3}$$

where $\nu_0 = 2{*}10^{10}$ Hz [51–55], T is the temperature, k_B is the Boltzmann constant. Similarly, the jumping frequency between $\theta_2 \rightarrow \theta_1$ states can be obtained as follows:

$$\nu_{21} = \nu_0\exp\left(-\frac{E_3 - E_2}{k_B T}\right) \tag{4}$$

5) If the magnetization of the nanoparticle was at the minimum θ_2 at a given moment, then the probability that it will be in the state corresponding to the minimum θ_1 one time step later is given by the following expression:

$$P_{21}\left(t_{step}\right) = \frac{\nu_{21}}{\nu_{12}+\nu_{21}}\left(1-\exp\left(-\left(\nu_{12}+\nu_{21}\right)t_{step}\right)\right) \tag{5}$$

and the probability corresponding to the transition $\theta_1 \rightarrow \theta_2$ is:

$$P_{12}\left(t_{step}\right) = \frac{\nu_{12}}{\nu_{12}+\nu_{21}}\left(1-\exp\left(-\left(\nu_{12}+\nu_{21}\right)t_{step}\right)\right) \tag{6}$$

Then, by generating a random number uniformly distributed between 0 and 1, and comparing the resulting value with the jump probability, it is decided whether a magnetization jumping occurs (The jump occurs in the plane spanned by the anisotropy axis of the given particle and the total magnetic field locally sensed by the particle). If not, the magnetization remains in the same state as in the previous step.

6) The magnetization values were obtained for each particle and finally average energy loss per particle was determined:

$$E_{loss} = \mu_0 M_s V \int_0^T \overline{H}_{ext} \frac{d\overline{m}}{dt} dt \tag{7}$$

7) The simulation was performed for 20 different initial configurations and these results were averaged.

Equation (7) gives the area of the hysteresis loop. The product of the energy loss per one cycle and the frequency of the excitation field is proportional to the specific loss power (SLP) or specific absorption rate (SAR):

$$E_{loss} f \propto SAR = SLP = \frac{\Delta T c}{t} \tag{8}$$

where ΔT is the temperature increment, c is the specific heat, and t is the time of the heating period. In order to compare the energy losses from experiments with different f and H values, it is more appropriate to use the reduced energy loss (ILP) [58,59]:

$$ILP = \frac{SAR}{H^2 f} \propto \frac{E_{loss}}{H^2} \tag{9}$$

in this work, the dimensionless energy loss we use is proportional to the ILP for constant field amplitude H:

$$\frac{E_{loss}}{2\pi\mu_0 M_s V H} \propto ILP \tag{10}$$

In the case of variable field strength, proportionality exists only if H^2 is present on the left side. It is important to note that the magnitude of the energy loss (the area of the hysteresis loop) is proportional to the phase delay between the magnetization vector and the external field. The kinetic Monte Carlo model is based on this assumption, because the anisotropy can be viewed as a barrier, which the magnetization has to overcome to jump from one state to the other.

The effect of the total magnetic field on the energy barrier is presented in Appendix I. The kinetic Monte Carlo was validated and the optimal time step size was determined for noninteracting particles in Appendix II.

We wanted to extend the results of our calculations based on the previous SLLG model [50,58] by taking anisotropy into account. This model was idealized/simplified, because we assumed noninteracting, isotropic MNPs. If we had taken into account the dipole-dipole interaction between the MNPs, then the CPU time would have increased dramatically. Therefore, in this work we use the kinetic Monte Carlo simulation which is suitable to describe these processes and requires much less computational time. The stochastic Landau-Lifshitz-Gilbert equation based model and the kinetic Monte Carlo model results could be compared well, which further validates the kinetic Monte Carlo model.

Let us now consider nanoparticles with the same size and material composition. To a first approximation, there is no interaction between the particles. Uniaxial anisotropy is assumed and the orientations of the particles are random. Particles are not able to mechanically rotate.

The magnitude of the external field/fields was compared to a reference field [56,57] in Refs. [50,58]. The magnitude of the reference field was $H_0 = 18\ kA/m$. The nanoparticle size and the saturation magnetization were $d_{mnp} = 20$ nm and $M_s = 640$ kA/m. If temperature and frequency were not variable parameters, then their values were fixed at 300K and 2 MHz. In the case of magnetite, depending on the shape, the value of the anisotropy energy density K varies between K = 10–20 kJ/m^3 [68]. In the kinetic Monte Carlo model, we first calculated with K = 10 kJ/m^3. When examining the dependence of energy loss on various parameters (frequency, temperature, static field), the amplitude of the oscillating and rotating field was adjusted to be equal to the anisotropy field calculated

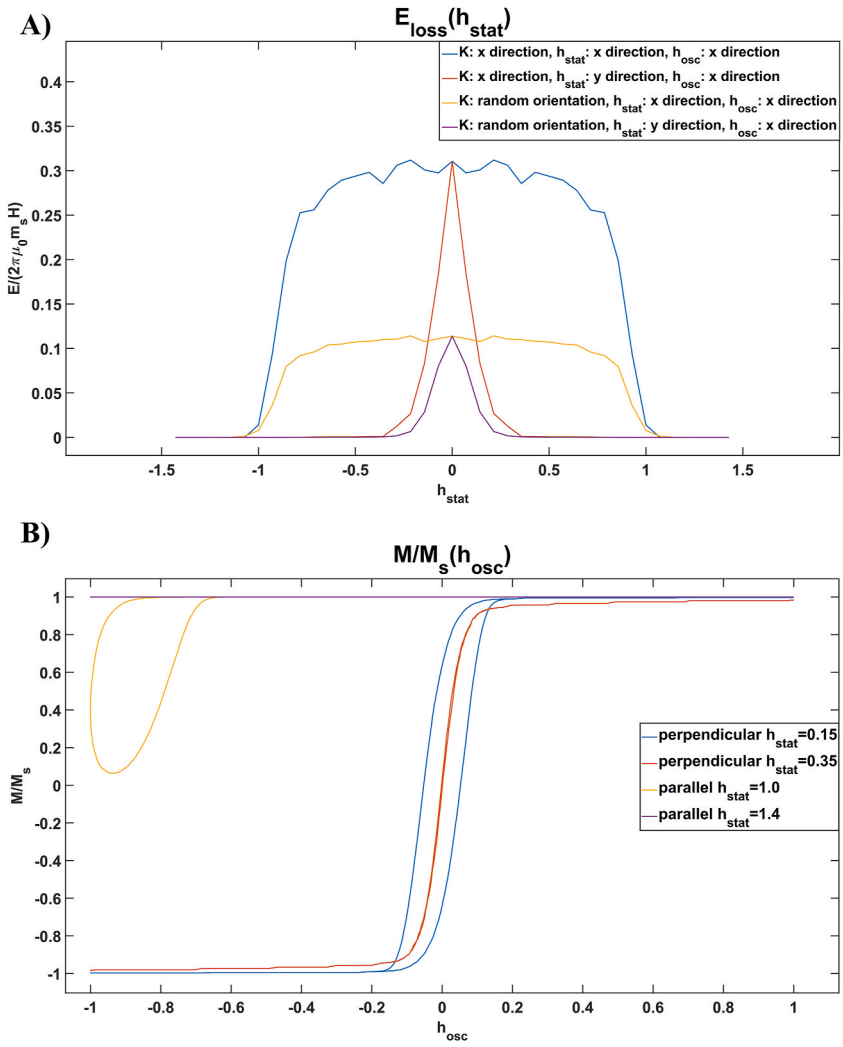

Fig. 2. (A) The energy loss per one cycle as a function of the static field (oscillating magnetic field with parallel and perpendicular static field, random orientation and x directional orientation) (B) The magnetization curves are shown below at different static fields.

from the K value. For uniaxial anisotropy, the anisotropy field can be obtained as follows [47]: $H_{ani} = \frac{2K}{\mu_0 M_s}$. Using this formula with the given parameters at K = 10 kJ/m^3, the anisotropy field is $H_{ani.ref} = 24.87\ kA/m = 1.3816\ H_0$ while the amplitude of the excitation field was adjusted to be the same $H = 24.87\ kA/m$. Let us also define the dimensionless ratios $h = \frac{H}{H_{ani.ref}}$ (which in this case is $h = 1$) and $h_{stat} = \frac{H_{stat}}{H_{ani.ref}}$. The anisotropy energy for these parameters is obtained to be KV = 4.2*10^{-20} J. The excitation fields can be written as follows:

$$H_{osc} = H(\cos(\omega t), 0, 0) \tag{11}$$

$$H_{rot} = H(\cos(\omega t), \sin(\omega t), 0) \tag{12}$$

$$H_{stat} = H(h_{stat}, 0, 0) \tag{13}$$

where H_{osc} , H_{rot} and H_{stat} are the oscillating, rotating and static fields. In the latter case the direction of the static field was altered in the different simulations.

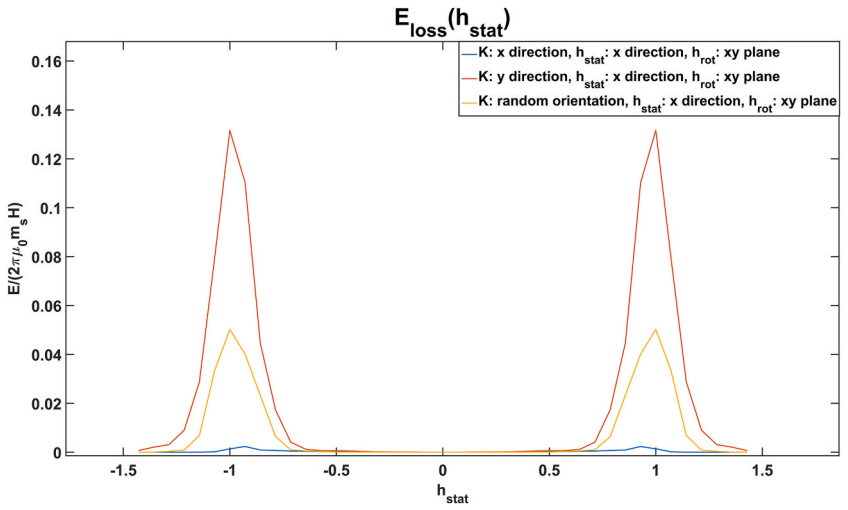

Fig. 3. The energy loss per one cycle as a function of the static field (rotating case). The peaks are present when the static field is in the plane of rotation.

3. Results and discussions

3.1. Spatial focusing in noninteracting systems

First a parallel or perpendicular static field was used in addition to the external oscillating field and we investigated the spatial focusing effect in Ref. [58]. It can be clearly seen (Fig. 2A.), that similar to the referenced article, in the case of a static magnetic field parallel to the oscillation, a wider energy curve is obtained, while in the perpendicular case, a narrower width energy curve is observed yielding a better localization effect. However, in both cases the energy curves are wider than in the referenced article. This may be due to the fact that they used isotropic nanoparticles there.

In order to understand the shape of the curves and the magnitude of the energy losses, the simulations were performed for cases where all the anisotropy axes were aligned in a given direction.

If the orientations of the nanoparticles are parallel to the direction of oscillation, then in both parallel and perpendicular cases, completely similar results are obtained as in cases with random orientation, only the magnitude of the energy loss is smaller. The results are shown at the top of Fig. 2.

If the oscillating field, the static field and the anisotropy axes are in the same direction, the results are the following. The bottom image (Fig. 2B) shows magnetization curves at two different static field values. Here, the static field was shown as a parameter in the diagrams, it was not added to the magnitude of the oscillating field on the horizontal axis. It can be clearly seen that the hysteresis gradually moves out by increasing the static field. When $h_{stat} > 1$, the static field is always larger than the oscillating one yielding a net external field that always points in the same direction. Thus, the magnetization vector also stays in this direction, see the purple line on the figure in case of $h_{stat} = 1.4$, where M/M_s is a constant and has a value close to one. This explains why the energy loss decreases at a slow rate at first and then shows a sudden drop when the hysteresis curve starts to disappear.

In the lower panel of the figure, one can see that the 2-dimensional area of the hysteresis curve quickly decreases with the increase of the static field in the perpendicular case as well. The faster decrease in energy loss, i.e., the narrower width energy curves can be understood by observing the fact that most of the energy loss comes from the time interval when the oscillating field decreases to zero and changes its sign. When a perpendicular field is added, the net external field is never zero and does not change its direction as quickly, resulting in a much smaller energy loss.

In cases where the orientation of the particles was perpendicular to the direction of the oscillating field, we obtained a magnetization curve without hysteresis typical of the heavy direction (in practice, we obtained an energy curve with orders of magnitude smaller). In these cases, it didn't matter which direction we set the static field, the energy loss was still zero.

We also investigated the effect of the rotating magnetic field and a static field parallel with or perpendicular to the plane of rotation. When applying a static field perpendicular to the plane of rotation, in the case of random orientation, we obtained a small and noisy energy function, which, like before, means practically zero losses. Adding a perpendicular static field does not show an increase in energy loss. This case is practically irrelevant for applications.

If the static field is in the plane of rotation, then two larger maxima are obtained (Fig. 3.). In Ref. [58], in the case of isotropic nanoparticles, two sharp maxima were observed when the magnitude of the static field and the amplitude of the rotating field were the same. In addition to the presence of anisotropy, we found that two peaks are also present (when the amplitude of the rotating field and the magnitude of the static field are the same), only wider than in the case of the isotropic nanoparticles in the referenced article.

Here, we also examined how much energy losses will be in the case of anisotropy axes set in a given direction. In the case of the combined application of a rotating magnetic field in the xy plane and a static field in the x direction, the following results were

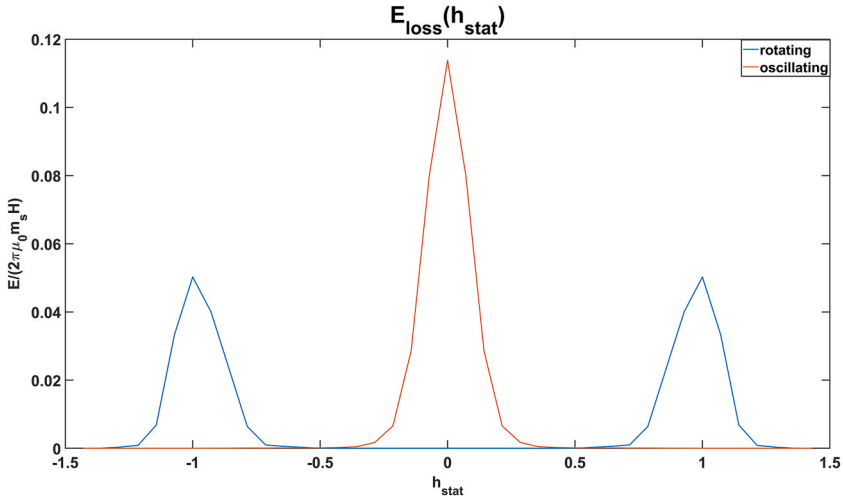

Fig. 4. Comparison of the energy loss as a function of the static field parameter for the oscillating and the rotating cases. The static field is perpendicular to the oscillation or parallel with the rotating plane.

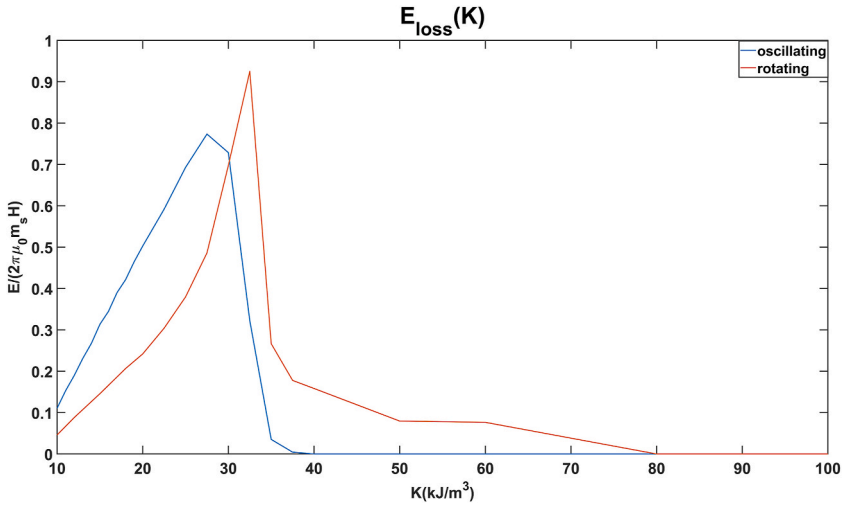

Fig. 5. The energy loss is shown as a function of the anisotropy energy density. It can be clearly seen that in the range 10–20 kJ/m^3 the loss is always larger in the oscillating field case. Above this, the loss increases in both cases, followed by a sharp decrease, only at different anisotropy energy densities.

obtained for nanoparticles aligned in the x direction. There are also two peaks when the amplitude of the rotating field is the same as the magnitude of the static field, but the rise from the 0 static field is more gradual than the decline for larger static fields. It can also be observed that the peaks are 1 order of magnitude smaller than in the case with random orientation. Thus, it can be said that the approach in this direction does not worsen the effect, but it certainly reduces its magnitude. Applying a rotating magnetic field in the XY plane and a static field in the x direction on nanoparticles oriented in the y direction has the following results. Two broader peaks appear again. They will also have their maxima at a static field of the same magnitude as the amplitude of the oscillating field. The shape of the curve of the energy loss function is the most similar to the case with random orientation, only here the losses are higher. The results for these are shown in Fig. 3.

For all other orientations, we obtained orders of magnitude smaller and noisier losses than the previous ones. As before, this means zero losses. Orientations in these directions clearly reduce the energy loss.

Finally, for the rest of this section we compared the two most important cases from the practical point of view (Fig. 4.): oscillating magnetic field with perpendicular static field and rotating magnetic field with parallel static field and random orientation for the anisotropy axis. It can be clearly seen that in the case of isotropic nanoparticles in Ref. [58], they reached a similar result to ours. In the case of an oscillating field, the energy loss is about twice as large as in the case of a rotating magnetic field. This is again due to the fact that most of the energy loss occurs when the net external field decreases to zero and quickly changes its direction. Since this happens twice in a cycle for the oscillating case while only once for the rotating one, the energy losses reflect this difference. See a more detailed

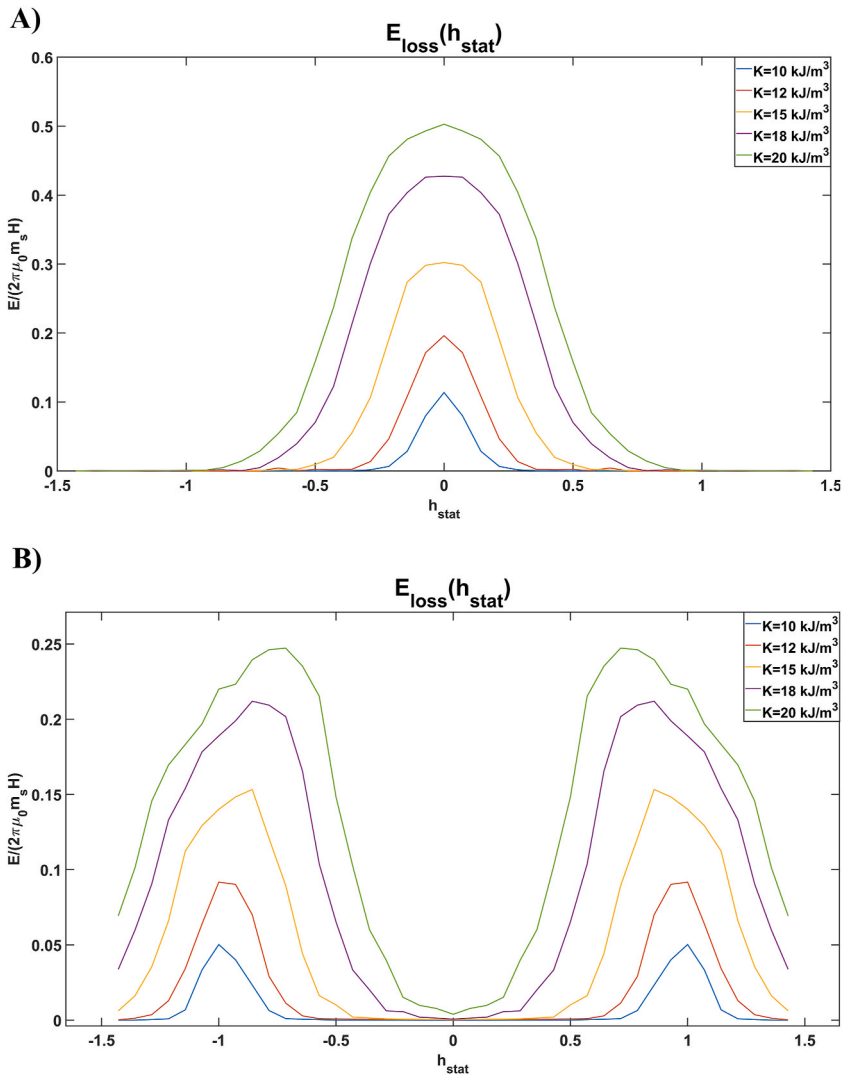

Fig. 6. The energy loss per one cycle as a function of the static field at different anisotropy energy densities ((A): oscillating and perpendicular static fields, (B): rotating and parallel static field fields; noninteracting systems). The peaks became wider, but the ratio of the maxima of the two cases did not change.

explanation in Ref. [58]. The difference compared to the isotropic case is the broadening of the peaks. Thus, although we cannot speak of such a good spatial focusing, anisotropic nanoparticles are still completely useable from a practical point of view.

Next, the anisotropy energy density dependence of energy loss was examined. The temperature was fixed at T = 300 K, the frequency at ω=2 MHz, and the saturation magnetization at M_s = 640,000 A/m. We did not change the amplitude of the oscillating and rotating field. Thus, we got an idea of the losses in the case of particles with an anisotropy field larger than the amplitude. It is important to note here that the losses were calculated at the peak values. However, as will be seen later, in the case of a rotating field, the peaks are shifted as the anisotropy increases. Thus, the anisotropy dependence of the energy loss in the rotating field was determined for each point at a different static field value, following the shift of the peaks. Fig. 5 shows the results. From a practical point of view, the range of 10–20 kJ/m3 applies to magnetite, as mentioned earlier. In this range, a linear increase is observed in both cases. However, with respect to the oscillating magnetic field, there is a steeper increase in the loss, and the relation between the oscillating and rotating field - namely that the peak of the energy loss for oscillating field is twice as large – still holds. The model assumes the presence of anisotropy by default. For this reason, the loss decreases as the barrier height approaches zero. And for very high anisotropy energy density, the energy loss also disappears. The latter phenomenon is confirmed in the literature for oscillating excitation fields [60–65]. For rotating magnetic fields, the loss starts to decrease at higher anisotropy energy densities and the peak value is also higher than for oscillating fields. This is an interesting result from a theoretical point of view, but for magnetite it is outside the range of the anisotropy energy density values observed in practice, as mentioned earlier.

After that, we looked at the static field dependence again, but with K = 10–20 kJ/m^3. In both cases, the peaks widened

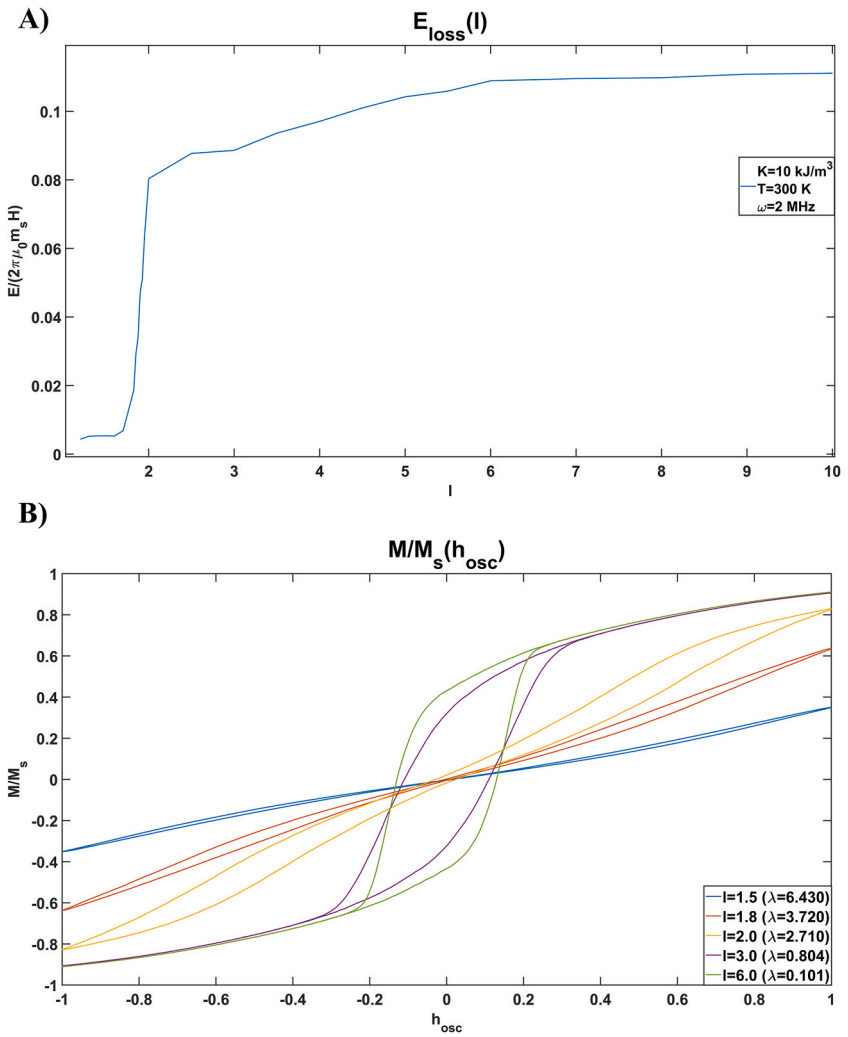

Fig. 7. The picture above (A) shows the l parameter dependence of the energy loss, and below (B) are the magnetization curves for some points.

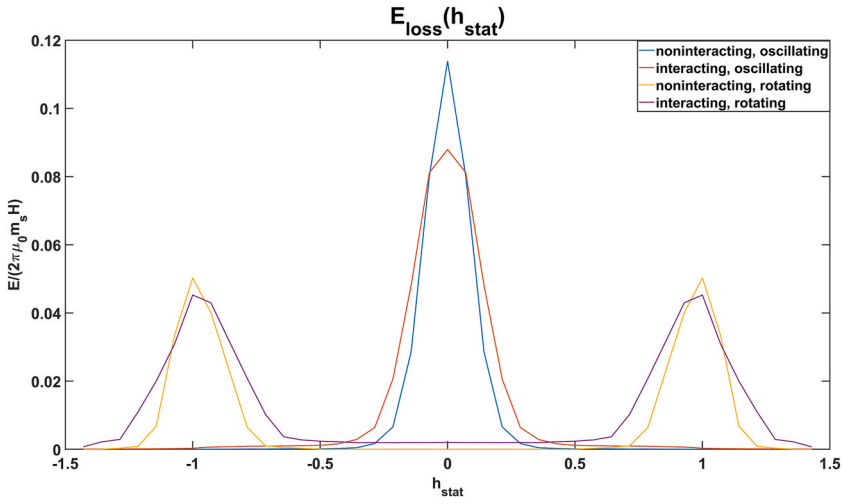

Fig. 8. The energy loss per one cycle as a function of the static field (rotating and oscillating field, interacting and noninteracting systems). The anisotropy energy density was K = 10 kJ/m^3.

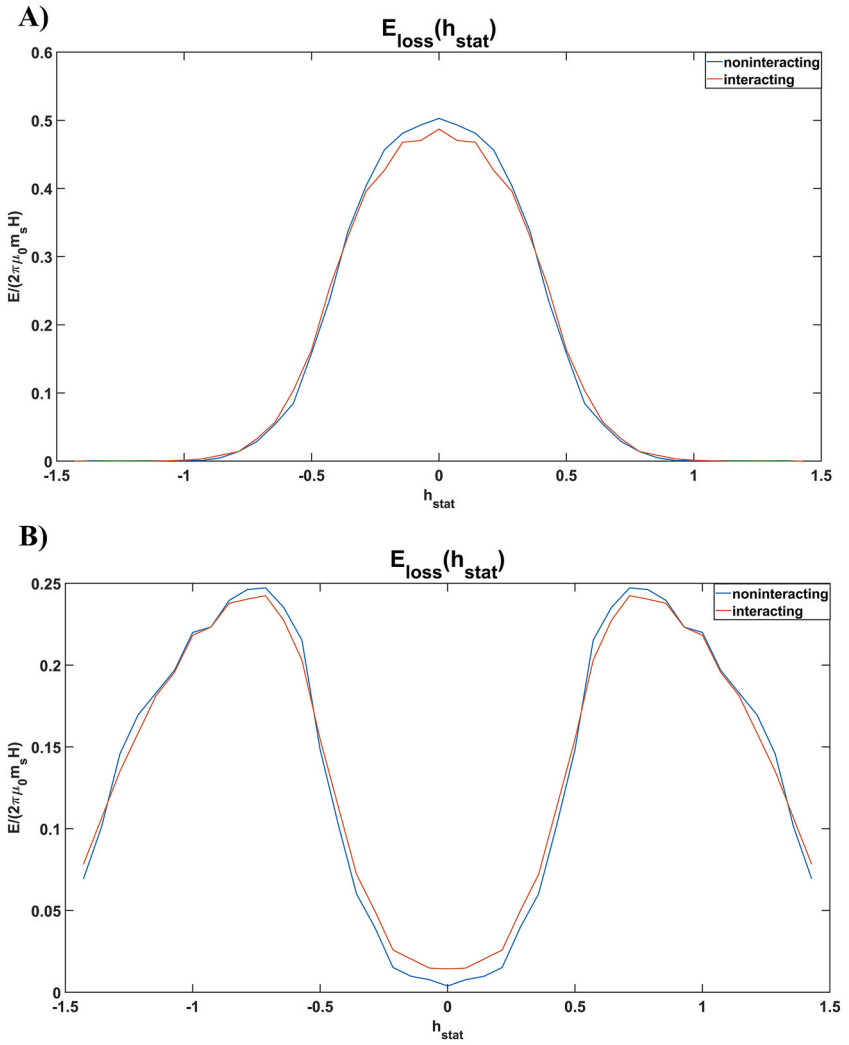

Fig. 9. At the top (A), the energy loss can be seen as a function of the static field parameter with the oscillating and perpendicular static field, and at the bottom (B) with the rotating and parallel static field. (K = 20 kJ/m^3).

considerably. On the other hand, the ratio of the peak values remained, with a loss of approximately twice as much in the oscillating field (see in Fig. 6.). In conclusion, for the applications in magnetic hyperthermia these simulations suggest that it could be advantageous to use nanoparticles with a larger anisotropy in the applicable range for magnetites. The disadvantage of this procedure would be the necessity to use larger gradients for the static field to obtain the same localization.

3.2. *Spatial focusing in interacting systems*

As a next step, the dipole-dipole interaction between the particles (Eq. (2)) was also taken into account. We placed the nanoparticles on a 10x10x10 cube lattice. This lattice is fully occupied with 1000 particles. Then moved their positions slightly randomly, i.e., by a random displacement smaller than the lattice size ($d_{mnp}/100$). Thus, overall, we got a randomized structure.

First of all, it is important to state that energy loss was always calculated for the second cycle, since the nanoparticles had not yet reached the "correct state" at the beginning of the first cycle. Thus, always only the energy loss of the second cycle was taken into account.

We first examined the effect of the interaction on the energy loss for nanoparticles at different distances in the oscillating field. The results are shown in Fig. 7. The lattice parameter l shown in the figure expresses the ratio between the distances between the centers of the nanoparticles and their diameter in case of a regular cubic lattice, i.e. the distance between the lattice points divided by the particle diameter. (during the simulations, a minimal random deviation was added to the position of the particles, so it is not regular). The lattice parameter was changed between l = 1.2 and l = 10, i.e. 24 nm and 200 nm. It can be clearly seen that the energy loss has a sharp decrease below a distance of approximately twice their diameter. For regions away from $l > 2$, a linear dependence can be observed,

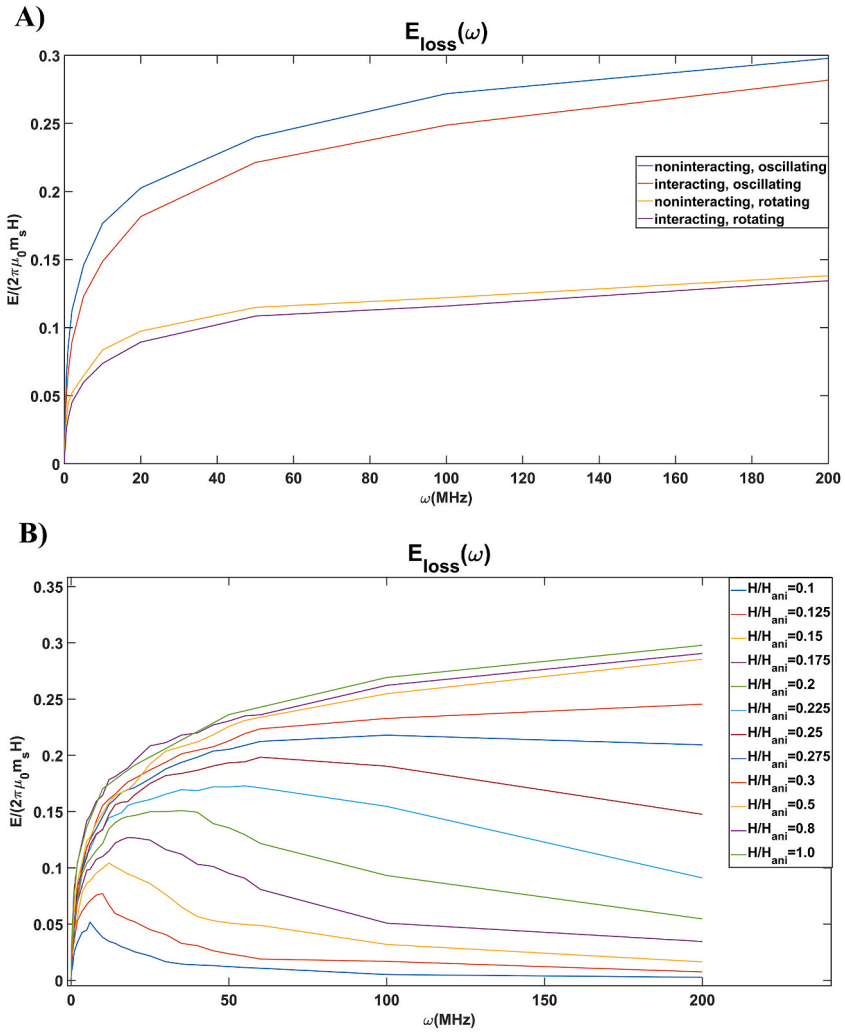

Fig. 10. At the top (A) one can see the energy loss per one cycle as a function of the angular frequency of the external field (oscillating or rotating, interacting or noninteracting). In the lower image (B), the energy loss can be seen at different amplitudes as a function of the angular frequency in the case of oscillating field in a noninteracting system.

while the energy loss tends to a constant in the large l limit recovering the non-interacting case. These $l > 6$ distance has also been given as a limit in the literature [65–67]. The strength of the interaction is often described by the following parameter, which is also shown in Fig. 7 [53,70].:

$$\lambda = \mu_0 M_s^2 V^2 \,/\, 4\pi \left(l d_{mnp}\right)^3 k_B T \tag{14}$$

After that, we examined the dependence of the energy loss on the static field in the case of particle distance $l = 3.0$ (Fig. 8). The results were compared with noninteracting cases. It can be clearly seen that the interaction has a similar effect on the energy loss in both cases of oscillating and rotating fields. There is a stronger decrease in the peak values, while the peaks have broadened. The former is more powerful in the oscillating case, while the latter is stronger in the case of the rotating fields.

If we increase the anisotropy energy density, the difference between interacting and noninteracting cases will be smaller. This is clearly seen in Fig. 9.

3.3. *Frequency and temperature dependence for interacting and noninteracting systems*

We examined the frequency dependence of the energy loss per cycle at oscillating and rotating excitation fields. As the frequency increases, the energy loss increases like the low frequency part of a Lorenz curve (Fig. 10A). Also in both cases, the interaction (with $l = 3.0$) reduces the energy loss throughout. In the lower part of the figure (Fig. 10B), it can be seen that if the amplitude is reduced, the energy loss increases for some time by increasing the frequency, and then decreases with further increasing of the frequency. The reason for this is that in the decreasing range the magnetization curve no longer reaches saturation, but instead becomes smaller and

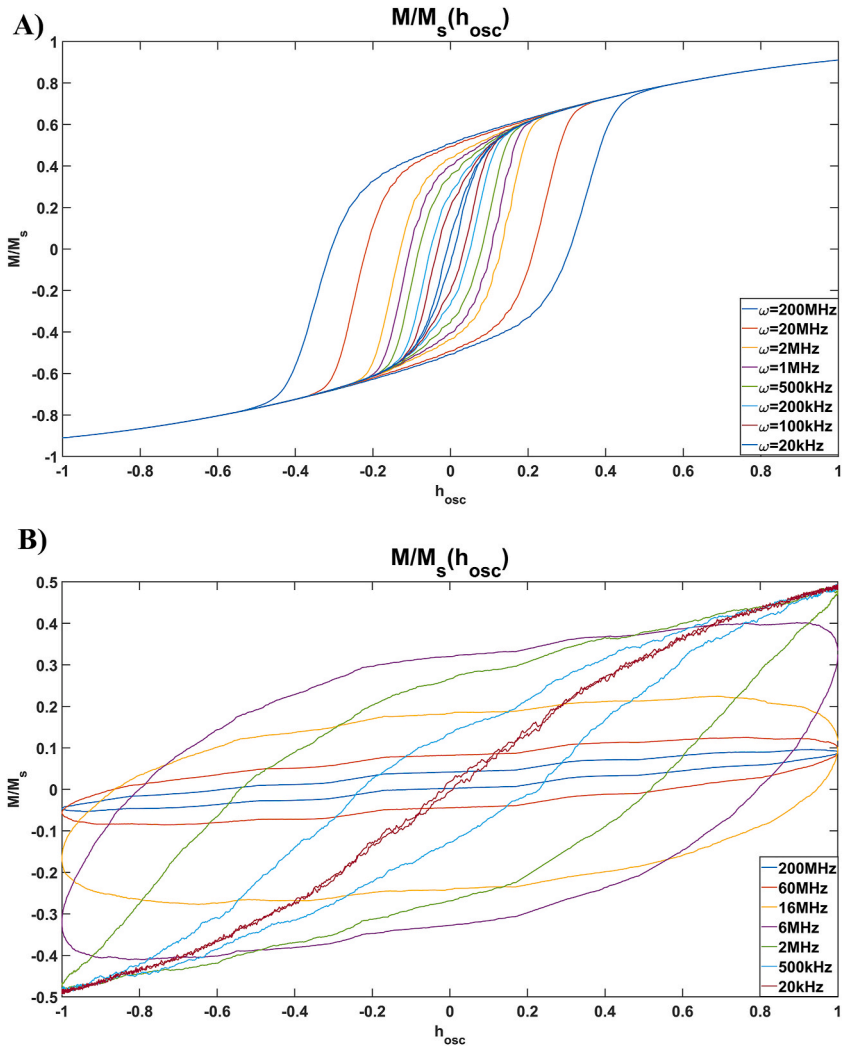

Fig. 11. The magnetization curves at different frequencies in noninteracting system ((A) top: h = 1 , (B) bottom: h = 0.1).

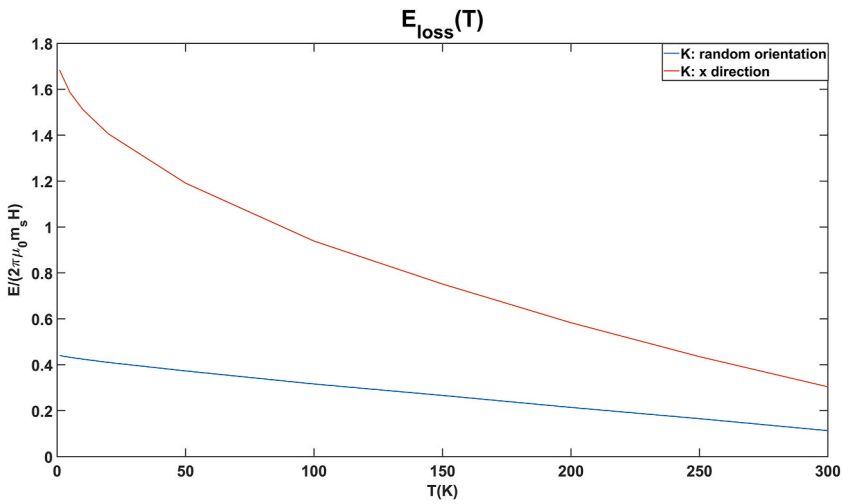

Fig. 12. The energy loss per one cycle as a function of the temperature (oscillating case, random orientation and x directional orientation).

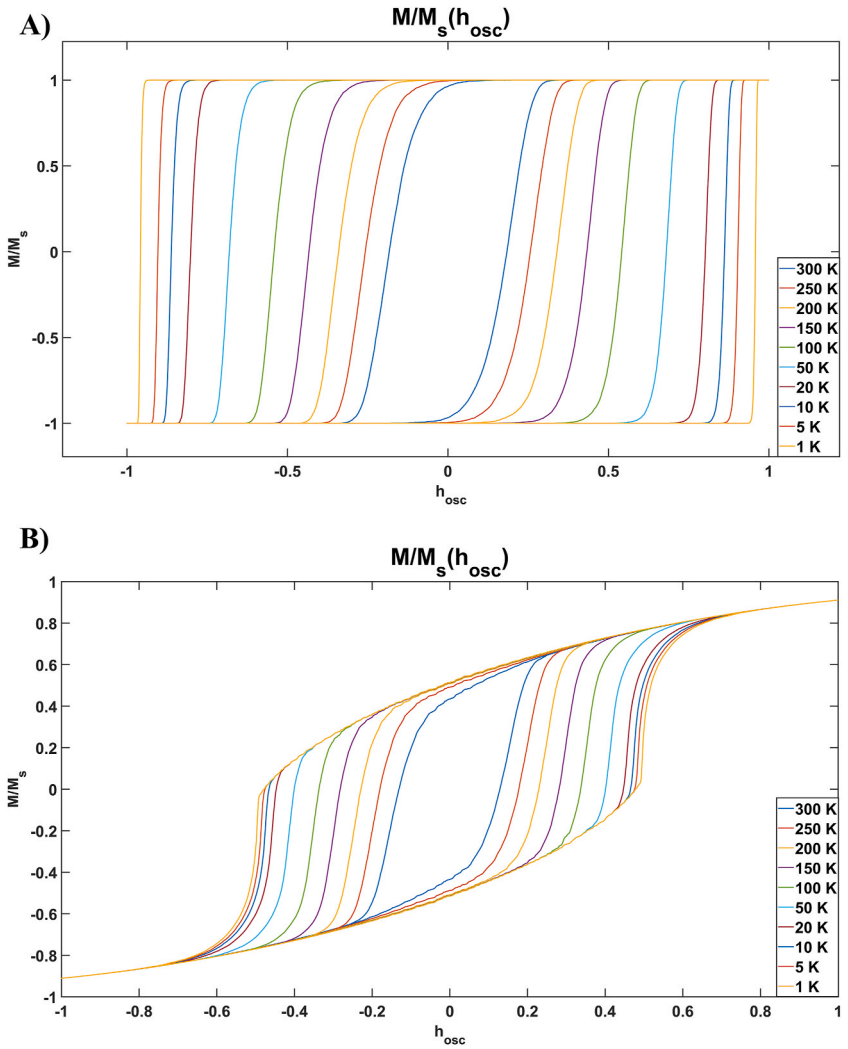

Fig. 13. The magnetization curves at different temperatures (oscillating case, x directional orientation (A) and random orientation (B)).

more elliptical in shape as shown in Fig. 11B. The elliptic magnetization curves and the Lorenz curve-like shape of the energy loss-frequency function that appeared in the fields of smaller amplitude are similar to the literatures [69,70].

Fig. 11 shows the magnetization curves calculated at different frequencies ((A) at $h = 1$ and (B) $h = 0.1$) in noninteracting system. In the first case, by increasing the frequency, the area of the hysteresis loop becomes larger and the magnetization reaches saturation. In the second case, by increasing the frequency, the area of the hysteresis loop becomes larger up to a certain value and the magnetization reaches saturation. However, by further increasing the frequency, the shape of the curve changes (the previously mentioned ellipse shape), the area of the hysteresis curve becomes smaller and the magnetization does not saturate.

Reference [58] also investigated the frequency dependence of the energy loss when applying oscillating or rotating magnetic field. The frequency dependence was examined at the peak values. The SLLG model in that article calculated with isotropic nanoparticles. In our case, the difference between the energy loss of the two types of excitation field is greater. This is due to the presence of anisotropy, and in the mentioned article there are several different parameters compared to the diffusion jump model. However, in terms of tendency, the results are similar.

Then the temperature dependence was examined. In Ref. [47], the effect of changing the temperature on the magnetization curve in the case of an external oscillating field was also investigated using the kinetic Monte Carlo method. According to the orientation of the particles, we run the simulations in two types of subbases: with random orientation and with anisotropy axes parallel to the direction of oscillation (in both cases there is no interaction between the nanoparticles). Although we did not run the program with exactly the same parameters as in the referenced article, the trend was similar. In the case of particles with the anisotropy axes in one direction, increasing and more angular shaped hysteresis loops appeared as the temperature decreased (see in Fig. 13A). If we examine randomly oriented nanoparticles, the area of the hysteresis curve also increases when the temperature is lowered, but here the magnetization curve is not square shaped and does not reach saturation (see in Fig. 13B). The reason for the difference in shape is that in the case of

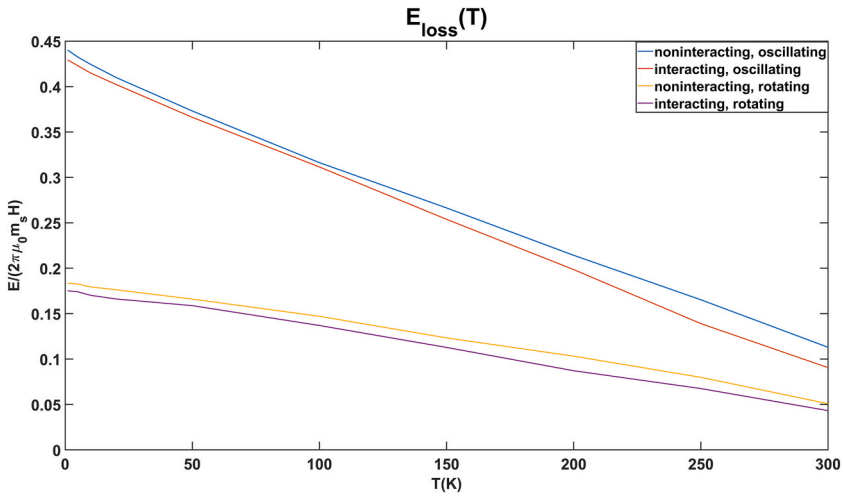

Fig. 14. The energy loss per one cycle as a function of the temperature (oscillating case (top), rotating case (bottom); interacting and noninteracting system).

particles with an anisotropy parallel to the oscillating field, magnetization occurs in the easy direction. In the case of random orientation, there will be particles in the system whose direction of the anisotropy axis differs from the easy direction, they may even be in the hard direction. There is no hysteresis loop for particles in hard direction. Thus, the totality of these gives the hysteresis curve of different size and shape experienced in the random orientation case compared to the unidirectional case. Fig. 12 shows that as the temperature increases, the energy loss decreases at a faster rate at lower temperatures in the case of unidirectional orientation, while in the case of random orientation, the loss decreases gradually as the temperature increases.

When examining the temperature dependence, it can also be seen that the interaction worsens the energy loss in both cases (Fig. 14.). At lower temperatures, the difference between interacting and non-interacting systems is smaller. It can be clearly seen that the effect of the interaction is smaller for a magnetic field oscillating at a lower temperature than at a higher temperature. No such tendency can be observed in the case of a rotating field.

4. Conclusions

In this article, we investigated whether the spatial focusing effect experienced in the case of isotropic, non-interacting particles in the case of rotating magnetic field and static field in the plane of rotation and in the case of oscillating magnetic field and static field perpendicular to oscillation is present for particles with anisotropy, and if they also interact. In our simulations we found that the energy loss increases with the increase of the anisotropy energy density in the applicable range for magnetites and the peaks become wider in both cases. In the case of a rotating magnetic field, it can also be observed that the location of the peaks is also shifted. If the nanoparticles also interact, the peaks flatten and widen in both cases. Taking all of this into account, it can be said that the presence of anisotropy has a positive effect from the standpoint of increasing the loss, but it significantly worsens the localization of the effect. The interaction between particles is not beneficial in any way in terms of energy loss.

From a practical point of view, for spatial focusing, it can therefore be said that it is necessary to strive to create particles with relatively small anisotropy and that do not interact with each other. There is a large drop in the energy loss when the distance is reduced to only twice of the diameter of the particles ($l = 2$), which must be avoided. Fortunately, if this ratio is around $l = 6$, then the results are already closely approximating the non-interacting case. When $2 < l < 6$ the energy loss is a bit reduced, but the spatial focusing effect still holds.

The time and frequency dependence of the energy loss was examined as well, recovering similar tendencies as in our previous article [58] validating both the applicability of the kinetic Monte-Carlo diffusion jump model, and the previous results obtained by the stochastic Landau-Lifshitz-Gilbert method. Based on the more realistic simulations performed in this work we can conclude that the spatial focusing effect and the frequency and temperature dependence of energy loss can be experimentally tested in real systems when the anisotropy and interaction between particles are present. Such experimental results are available for oscillating fields, but the enhancement of energy loss in the combined linear and rotating field was experimentally not studied.

Data availability statement

No data was used for the research described in the article.

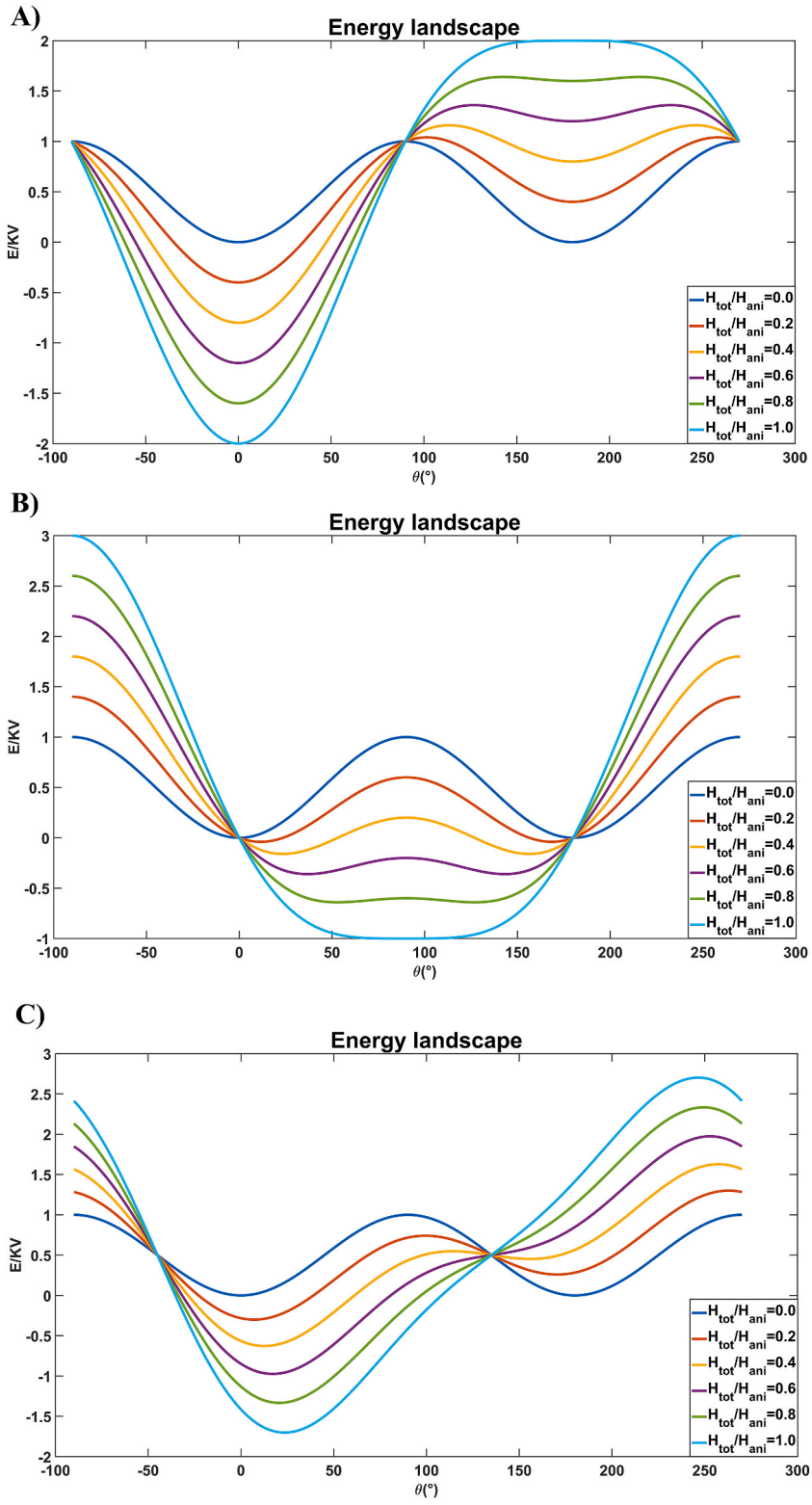

Fig. 15. The energy of single nanoparticle as a function of theta at different total magnetic field strengths. In the top image (A), the angle is 0° between the total magnetic field and the anisotropy axis. The 90-degree case is shown in the middle image (B), and the 45-degree case is shown below (C).

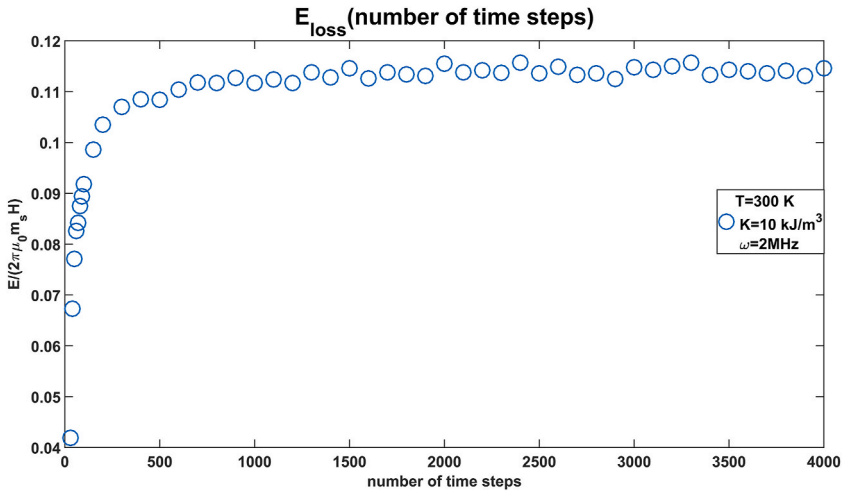

Fig. 16. The energy loss per one cycle as a function of the number of time steps. The energy loss is saturated above 1000 time steps.

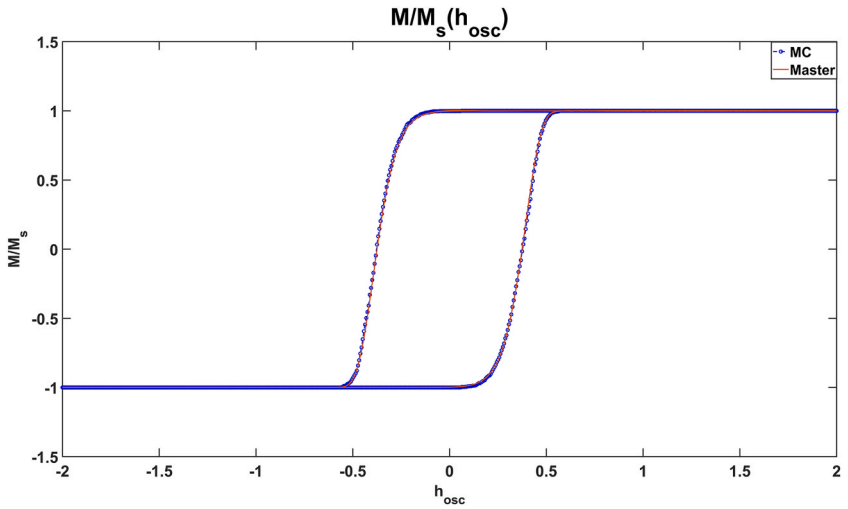

Fig. 17. Comparison of simulations based on the kinetic Monte Carlo method and the Master equation. The nanoparticle size is 20 nm and the anisotropy energy density is 10 kJ/m^3 and the angular frequency is 20 MHz. The results of the two models completely overlap.

CRediT authorship contribution statement

Vilmos Vékony: Writing – original draft, Software, Investigation, Conceptualization. **István G. Márián:** Writing – review & editing, Supervision, Conceptualization. **István A. Szabó:** Writing – review & editing, Supervision, Conceptualization.

Declaration of competing interest

The authors declare that they have no known competing financial interests or personal relationships that could have appeared to influence the work reported in this paper.

Acknowledgement

The authors thank the GINOP-2.3.2-15-2016-00041 Regional Materials Science Excellence Workshop - Research Program and Infrastructure tender for the financial support. The support of the ED_18-1-2019-0028 Thematic Excellence Program is gratefully acknowledged.

6.1. Appendix I. Energy states

Fig. 15 shows the energy states of a given particle in relation to the anisotropy axis according to different directions of magnetization. If the particle does not sense an external magnetic field and no dipole field from interactions is present, then two minima are observed, at 0 and 180°. On the other hand, if the total magnetic field is not 0 and it is in the same direction as the anisotropy axis, then the minimum opposite to the direction of the field rises and the other decreases (see in Fig. 15A). The lower one, i.e. the minimum corresponding to the direction of field, will be the more stable state. If the magnitude of the total external magnetic field reaches the magnitude of the anisotropy field, there will be only one minimum. If the direction of the entire magnetic field is perpendicular to the anisotropy axis, then by increasing the field, it can be seen that there will always be 2 minima of the same depth until the external field strength corresponding to the size of the anisotropy field is reached (see in Fig. 15B). The location of these minima also changes. As the field increases, the direction of the magnetization vector deviates more and more from the anisotropy axis to the direction of the magnetic field. Below, the magnetic field and the anisotropy axis enclose 45° (see in Fig. 15C). It can be clearly seen that the locations of the minimums and their relative sizes also change with increasing magnetic field. Here, however, even in the case of the total magnetic field smaller than the anisotropy field, it is possible to achieve only one energy minimum.

6.2. Appendix II. Validation of the kinetic Monte Carlo method

First, the effect of the number of the time steps per cycle was investigated on the energy loss. The periodic time was determined from the frequency of the external magnetic field, and then such a time interval was divided into n time steps. The results are shown in Fig. 16. The simulations were running in noninteracting system and the anisotropy axes of the nanoparticles were parallel with the external magnetic field. The temperature was 300 K, the angular frequency of the external magnetic field was 2 MHz and the anisotropy energy density was 10 kJ/m^3. An optimal value of the number of time steps was sought, where the energy loss does not change if the magnetization process was divided into even finer parts and the CPU time is not too high. It can be clearly seen that the energy loss is saturated above 1000 time steps. Therefore, we used later 2000 time steps, like in the literature [49].

The diffusion jump behavior of magnetization can also be modelled by another method. This other method is based on the Master equation. The differential equations for the state probabilities of the magnetization states will be as follows:

$$\frac{dp_i}{dt} = -p_i(\nu_{12} + \nu_{21}) + \nu_{ji} \tag{15}$$

The axial projection of the magnetization anisotropy can be obtained as follows [47]:

$$M = M_s(p_1 \cos(\theta_1) + (1 - p_1)\cos(\theta_2)) \tag{16}$$

Using equations (7) and (15), the energy loss per one cycle can be obtained as follows:

$$E = 2\mu_0 M_s V \int_0^T H_{ext}(t)(p_1\nu_{12} - p_2\nu_{21})\, dt \tag{17}$$

So we compared the results of the Master equation with the results of the kinetic Monte Carlo simulation. In the former case, we ran the simulation for one particle for 10 cycles. In the latter case, we ran the simulation for 1000 particles over 2 cycles (here the particles had their anisotropy axis direction the same and aligned with the external magnetic field). In the kinetic Monte Carlo simulations, a cycle starts at the (positive) maximum of the external field, then reaches the (negative) minimum value and the excitation field increases in the same way backwards. At the beginning of the first cycle, there are nanoparticles that are not fully saturated, so the hysteresis loop at the beginning of the next cycle does not return to the value at the beginning of the first cycle. Therefore, the first cycle was not considered, only the second cycle was left (this is true for all simulations). The comparison is shown in Fig. 17. The two models produce sufficiently similar results.

References

[1] D. Ortega, Q.A. Pankhurst, Magnetic hyperthermia, Nanoscience 1 (2013) 60–88, https://doi.org/10.1039/9781849734844-00060.

[2] A. Rajan, N.K. Sahu, Review on magnetic nanoparticle-mediated hyperthermia for cancer therapy, J. Nanoparticle Res. 22 (2020) 319, https://doi.org/10.1007/s11051-020-05045-9.

[3] D. Chang, M. Lim, J.A.C.M. Goos, R. Qiao, Y.Y. Ng, F.M. Mansfeld, M. Jackson, T.P. Davis, M. Kavallaris, Biologically targeted magnetic hyperthermia: potential and limitations, frontiers in pharmacology sec, Drugs Outcomes Research and Policies 9 (2018) 831, https://doi.org/10.3389/fphar.2018.00831.

[4] E.A. Périgo, G. Hemery, O. Sandre, D. Ortega, E. Garaio, F. Plazaola, F.J. Teran, Fundamentals and advances in magnetic hyperthermia, Appl. Phys. Rev. 2 (4) (2015) 041302, https://doi.org/10.1063/1.4935688.

[5] L. Kafrouni, O. Savadogo, Recent progress on magnetic nanoparticles for magnetic hyperthermia, Progress in Biomaterials 5 (2016) 147–160, https://doi.org/10.1007/s40204-016-0054-6.

[6] M. Peiravi, H. Eslami, M. Ansari, H. Zare-Zardini, Magnetic hyperthermia: potentials and limitations, J. Indian Chem. Soc. 99 (1) (2022) 100269, https://doi.org/10.1016/j.jics.2021.100269. ISSN 0019-4522.

[7] O.R. Farzam, N. Mehran, F. Bilan, E. Aghajani, R. Dabbaghipour, G.A. Shahgoli, B. Baradaran, Nanoparticles for imaging-guided photothermal therapy of colorectal cancer, Heliyon 9 (11) (2023) e21334, https://doi.org/10.1016/j.heliyon.2023.e21334.

[8] M. Arif, A.F. Nawaz, S. Ullah khan, H. Mueen, F. Rashid, H.A. Hemeg, A. Rauf, Nanotechnology-based radiation therapy to cure cancer and the challenges in its clinical applications, Heliyon 9 (6) (2023) e17252, https://doi.org/10.1016/j.heliyon.2023.e17252.

[9] B.K. Najafabad, N. Attaran, M. Barati, Z. Mohammadi, M. Mahmoudi, A. Sazgarnia, Cobalt ferrite nanoparticle for the elimination of CD133+CD44^{+} and CD44^{+}CD24^{-}, in breast and skin cancer stem cells, using non-ionizing treatments, Heliyon 9 (10) (2023) e19893, https://doi.org/10.1016/j.heliyon.2023.e19893.

[10] G.P. Skandalakis, D.R. Rivera, C.D. Rizea, A. Bouras, J.G.J. Raj, D. Bozec, C.G. Hadjipanayis, Hyperthermia treatment advances for brain tumors, Int. J. Hyperther. 37 (2) (2020) 3–19, https://doi.org/10.1080/02656736.2020.1772512.

[11] C. Wang, Chao-Hsiung Hsu, Z. Li, Lian-Pin Hwang, Ying-Chih Lin, Pi-Tai Chou, Yung-Ya Lin, Effective heating of magnetic nanoparticle aggregates for in vivo nano-theranostic hyperthermia, Int. J. Nanomed. 12 (2017) 6273–6287, https://doi.org/10.2147/IJN.S141072.

[12] P. Ilg, M. Kröger, Field- and concentration-dependent relaxation of magnetic nanoparticles and optimality conditions for magnetic fluid hyperthermia, Sci. Rep. 13 (2023) 16523, https://doi.org/10.1038/s41598-023-43140-8.

[13] S. Guba, B. Horváth, I. Szalai, Application and comparison of thermistors and fiber optic temperature sensor reference for ILP measurement of magnetic fluids in double cell magnetic hyperthermia, Heliyon 8 (6) (2022) e09606, https://doi.org/10.1016/j.heliyon.2022.e09606.

[14] D. Khan, A. ur Rahman, P. Kumam, W. Watthayu, K. Sitthithakerngkiet, A.M. Galal, Thermal analysis of different shape nanoparticles on hyperthermia therapy on breast cancer in a porous medium: a fractional model, Heliyon 8 (8) (2022) e10170, https://doi.org/10.1016/j.heliyon.2022.e10170.

[15] L.M. Al-Harbi, M.S.A. Darwish, Functionalized iron oxide nanoparticles: synthesis through ultrasonic-assisted co-precipitation and performance as hyperthermic agents for biomedical applications, Heliyon 8 (6) (2022) e09654, https://doi.org/10.1016/j.heliyon.2022.e09654.

[16] S. Gao, M. Zheng, X. Ren, Y. Tang, X. Liang, Local hyperthermia in head and neck cancer: mechanism, application and advance, Oncotarget 7 (35) (2016) 57367–57378, 10.18632%2Foncotarget.10350.

[17] V.E. Kouloulias, C.E. Dardoufas, J.R. Kouvaris, C.S. Gennatas, A.K. Polyzos, H.J. Gogas, P.H. Sandilos, N.K. Uzunoglu, E.G. Malas, L.J. Vlahos, Liposomal doxorubicin in conjunction with reirradiation and local hyperthermia treatment in recurrent breast cancer: a phase I/II trial, Clin. Cancer Res. 8 (2) (2002) 374–382.

[18] R. Hergt, S. Dutz, Magnetic particle hyperthermia—biophysical limitations of a visionary tumour therapy, J. Magn. Magn Mater. 311 (2007) 187–192, https://doi.org/10.1016/j.jmmm.2006.10.1156.

[19] Q.A. Pankhurst, J. Connolly, S.K. Jones, J. Dobson, Applications of magnetic nanoparticles in biomedicine, J. Phys. D Appl. Phys. 36 (2003) R167–R181, https://doi.org/10.1088/0022-3727/36/13/201.

[20] S. Hayek, C.J. Chen, Y. Haik, V. Mohite, Application of nanomagnetic particles in hyperthermia cancer treatment, NSTI-Nanotech 2006 Technical Proceedings 2 (2006) 67–70.

[21] V.N. Nikiforov, Magnetic induction hyperthermia, Russ. Phys. J. 50 (2007) 913–924, https://doi.org/10.1007/s11182-007-0133-1.

[22] E.C. Abenojar, S. Wickramasinghe, J. Bas-Concepcion, A.C.S. Samia, Structural effects on the magnetic hyperthermia properties of iron oxide nanoparticles, Prog. Nat. Sci.: Mater. Int. 26 (2016) 440–448, https://doi.org/10.1016/j.pnsc.2016.09.004.

[23] S.M. Cassim, A.J. Giustini, A.A. Petryk, R.A. Strawbridge, P.J. Hoopes, Iron oxide nanoparticle hyperthermia and radiation cancer treatment, proceedings 7181, energy-based treatment of tissue and assessment V; 71810O. https://doi.org/10.1117/12.810035, 2009.

[24] S. Laurent, S. Dutz, U.O. Häfeli, M. Mahmoudi, Magnetic fluid hyperthermia: focus on superparamagnetic iron oxide nanoparticles, Adv. Colloid Interface Sci. 166 (2011) 8–23, https://doi.org/10.1016/j.cis.2011.04.003.

[25] P. Ilg, Diffusion-jump model for the combined Brownian and Néel relaxation dynamics of ferrofluids in the presence of external fields and flow, Phys. Rev. 100 (2) (2019) 022608, https://doi.org/10.1103/PhysRevE.100.022608. ISSN 15393755.

[26] T. Gabriel, Landi, Role of dipolar interaction in magnetic hyperthermia, Phys. Rev. B 89 (2014) 014403, https://doi.org/10.1103/PhysRevB.89.014403.

[27] D.F. Coral, P.M. Zélis, M. Marciello, M.D.P. Morales, A. Craievich, F.H. Sanchez, M.B.F. van Raap, On the effect of nanoclustering and dipolar interactions in heat generation for magnetic hyperthermia, Langmuir 32 (5) (2016) 1201–1213, https://doi.org/10.1021/acs.langmuir.5b03559.

[28] I. Conde-Leborán, D. Serantes, D. Baldomir, Orientation of the magnetization easy axes of interacting nanoparticles: influence on the hyperthermia properties, J. Magn. Magn Mater. 380 (2015) 321–324, https://doi.org/10.1016/j.jmmm.2014.10.022.

[29] M. Anand, V. Banerjee, J. Carrey, Relaxation in one-dimensional chains of interacting magnetic nanoparticles: analytical formula and kinetic Monte Carlo simulations, Phys. Rev. B 99 (2019) 024402, https://doi.org/10.1103/PhysRevB.99.024402.

[30] N.A. Usov, O.N. Serebryakova, V.P. Tarasov, Interaction effects in assembly of magnetic nanoparticles, Nanoscale Res. Lett. 12 (2017) 489, https://doi.org/10.1186/s11671-017-2263-x.

[31] N.A. Usov, M.S. Nesmeyanov, E.M. Gubanova, N.B. Epshtein, Heating ability of magnetic nanoparticles with cubic and combined anisotropy, Beilstein J. Nanotechnol. 10 (2019) 305–314, 10.3762%2Fbjnano.10.29.

[32] U.M. Engelmann, C. Shasha, E. Teeman, I. Slabu, K.M. Krishnan, Predicting size-dependent heating efficiency of magnetic nanoparticles from experiment and stochastic Néel-Brown Langevin simulation, J. Magn. Magn Mater. 471 (2019) 450–456, https://doi.org/10.1016/j.jmmm.2018.09.041.

[33] R. Fu, Y. Yan, C. Roberts, Z. Liu, Y. Chen, The role of dipole interactions in hyperthermia heating colloidal clusters of densely-packed superparamagnetic nanoparticles, Sci. Rep. 8 (2018) 4704, https://doi.org/10.1038/s41598-018-23225-5.

[34] P.W. Egolf, N. Shamsudhin, S. Pané, D. Vuarnoz, J. Pokki, Anne Gabrielle Pawlowski, P. Tsague, B. de Marco, W. Bovy, S. Tucev, M.H.D. Ansari, B.J. Nelson, Hyperthermia with rotating magnetic nanowires inducing heat into tumor by fluid friction, J. Appl. Phys. 120 (2016) 064304, https://doi.org/10.1063/1.4960406.

[35] P. Cantillon-Murphy, L.L. Wald, M. Zahn, E. Adalsteinsson, Proposing magnetic nanoparticle hyperthermia in low-field MRI, Concepts Magn. Reson. 36A (1) (2010) 36–47, https://doi.org/10.1002/cmr.a.20153.

[36] J. Dieckhoff, M. Schilling, F. Ludwig, Magnetic marker based homogeneous bioassays utilizing rotating magnetic fields, J. Appl. Phys. 115 (2014) 17B304, https://doi.org/10.1063/1.4862943.

[37] Z.M. Sherman, J.L. Pallone, R.M. Erbb, J.W. Swan, Enhanced diffusion and magnetophoresis of paramagnetic colloidal particles in rotating magnetic fields, Soft Matter 15 (2019) 6677–6689, https://doi.org/10.1039/C9SM00890J.

[38] B. Mehdaoui, J. Carrey, M. Stadler, A. Cornejo, C. Nayral, F. Delpech, B. Chaudret, M. Respaud, Influence of a transverse static magnetic field on the magnetic hyperthermia properties and high-frequency hysteresis loops of ferromagnetic FeCo nanoparticles, Appl. Phys. Lett. 100 (2012) 052403, https://doi.org/10.1063/1.3681361.

[39] E. Myrovali, N. Maniotis, T. Samaras, M. Angelakeris, Spatial focusing of magnetic particle hyperthermia, Nanoscale Adv. 2 (2020) 408, https://doi.org/10.1039/C9NA00667B.

[40] R. Onodera, E. Kita, M. Kishimoto, T. Kuroiwa, H. Yanagihara, Dynamic hysteresis measurement of magnetic nano particle suspensions in parallel and perpendicular DC magnetic fields, IEEE Trans. Magn. 57 (2) (2021), https://doi.org/10.1109/TMAG.2020.3021428.

[41] P.M. Déjardin, Yu P. Kalmykov, B.E. Kashevsky, H. El Mrabti, I.S. Poperechny, Yu L. Raikher, S.V. Titov, Effect of a dc bias field on the dynamic hysteresis of single-domain ferromagnetic particles, J. Appl. Phys. 107 (2010) 073914, https://doi.org/10.1063/1.3359722.

[42] H. El Mrabti, S.V. Titov, P.-M. Déjardin, Y.P. Kalmykov, Nonlinear stationary ac response of the magnetization of uniaxial superparamagnetic nanoparticles, J. Appl. Phys. 110 (2011) 023901, https://doi.org/10.1063/1.3605536.

[43] K. Murase, A simulation study on the specific loss power in magnetic hyperthermia in the presence of a static magnetic field, Open J. Appl. Sci. 6 (2016) 839–851, https://doi.org/10.4236/ojapps.2016.612073.

[44] R. Dhavalikar, C. Rinaldi, Theoretical predictions for spatially-focused heating of magnetic nanoparticles guided by magnetic particle imaging field gradients, J. Magn. Magn Mater. 419 (2016) 267–273, https://doi.org/10.1016/j.jmmm.2016.06.038.

[45] R.A. Rytov, N.A. Usov, Specific absorption rate of randomly oriented magnetic nanoparticles in a static magnetic field, Beilstein J. Nanotechnol. 14 (2023) 485–493, https://doi.org/10.3762/bjnano.14.39.

[46] Z. Zhao, C. Rinaldi, Magnetization dynamics and energy dissipation of interacting magnetic nanoparticles in alternating magnetic fields with and without A static bias field, J. Phys. Chem. C 122 (36) (2018) 21018–21030, https://doi.org/10.1021/acs.jpcc.8b04071.

[47] J. Carrey, B. Mehdaoui, M. Respaud, Simple models for dynamic hysteresis loop calculations of magnetic single-domain nanoparticles: application to magnetic hyperthermia optimization, J. Appl. Phys. 109 (2011) 083921, https://doi.org/10.1063/1.3551582.
[48] C. Papadopoulos, A. Kolokithas-Ntoukas, R. Moreno, D. Fuentes, G. Loudos, V.C. Loukopoulos, G.C. Kagadis, Using kinetic Monte Carlo simulations to design efficient magnetic nanoparticles for clinical hyperthermia, Med. Phys. 49 (1) (2022) 547–567, https://doi.org/10.1002/mp.15317.
[49] R.P. Tan, J. Carrey, M. Respaud, Magnetic hyperthermia properties of nanoparticles inside lysosomes using kinetic Monte Carlo simulations: influence of key parameters and dipolar interactions, and evidence for strong spatial variation of heating power, Phys. Rev. B 90 (2014) 214421, https://doi.org/10.1103/PhysRevB.90.214421.
[50] Zs Iszály, K. Lovász, I. Nagy, I.G. Márián, J. Rácz, I.A. Szabó, L. Tóth, N.F. Vas, V. Vékony, I. Nándori, Efficiency of magnetic hyperthermia in the presence of rotating and static fields, J. Magn. Magn Mater. 466 (2018) 452–462, https://doi.org/10.1016/j.jmmm.2018.07.043.
[51] S. Yoon, Determination of the temperature dependence of the magnetic anisotropy constant in magnetite nanoparticles, J. Kor. Phys. Soc. 59 (5) (2011) 3069–3073, https://doi.org/10.3938/jkps.59.3069.
[52] F. Luis, J.M. Torres, L.M. García, J. Bartolomé, J. Stankiewicz, F. Petroff, F. Fettar, J.-L. Maurice, A. Vaurès, Enhancement of the magnetic anisotropy of nanometer-sized Co clusters: influence of the surface and of interparticle interactions, Phys. Rev. B 65 (2002) 094409, https://doi.org/10.1103/PhysRevB.65.094409.
[53] D. Sarkar, M. Mandal, Static and dynamic magnetic characterization of DNA-templated chain-like magnetite nanoparticles, J. Phys. Chem. C 116 (5) (2012) 3227–3234, https://doi.org/10.1021/jp208020z.
[54] X.X. Zhang, Magnetic relaxation and quantum tunneling of magnetization, in: Y. Liu, D.J. Sellmyer, D. Shindo (Eds.), Handbook of Advanced Magnetic Materials, Springer, Boston, MA, 2006, https://doi.org/10.1007/1-4020-7984-2_5.
[55] A. Rostamnejadi, H. Salamati, P. Kameli, H. Ahmadvand, Superparamagnetic behavior of $La_{0.67}Sr_{0.33}MnO_3$ nanoparticles prepared via sol–gel method, J. Magn. Magn Mater. 321 (2009) 3126–3131, https://doi.org/10.1016/j.jmmm.2009.05.035.
[56] U. Gneveckow, A. Jordan, R. Scholz, V. Bruss, N. Waldofner, J. Ricke, A. Feussner, B. Hildebrandt, B. Rau, P. Wust, Description and characterization of the novel hyperthermia and thermoablation system for clinical magnetic fluid hyperthermia, Med. Phys. 31 (2004) 1444–1451, https://doi.org/10.1118/1.1748629.
[57] B. Thiesen, A. Jordan, Clinical applications of magnetic nanoparticles for hyperthermia, Int. J. Hyperther. 24 (2008) 467–474, https://doi.org/10.1080/02656730802104757.
[58] Zs Iszály, I.G. Márián, I.A. Szabó, A. Trombettoni, I. Nándori, Theory of superlocalized magnetic nanoparticle hyperthermia: rotating versus oscillating fields, J. Magn. Magn Mater. 541 (2022) 168528, https://doi.org/10.1016/j.jmmm.2021.168528.
[59] Zs Iszály, I. Gresits, I.G. Márián, Gy Thuróczy, O. Sági, B.G. Márkus, F. Simon, I. Nándori, Polarized superlocalization in magnetic nanoparticle hyperthermia, J. Phys. Appl. Phys. 55 (2022) 205001, https://doi.org/10.1088/1361-6463/ac526d.
[60] H. Jalili, B. Aslibeiki, A. Ghotbi Varzaneh, V.A. Chernenko, The effect of magneto-crystalline anisotropy on the properties of hard and soft magnetic ferrite nanoparticles, Beilstein J. Nanotechnol. 10 (2019) 1348–1359, 10.3762%2Fbjnano.10.133.
[61] U.M. Engelmann, Assessing Magnetic Fluid Hyperthermia: Magnetic Relaxation Simulation, Modeling of Nanoparticle Uptake inside Pancreatic Tumor Cells and in Vitro Efficacy, first ed., Infinite Science Publishing: Lübeck, Germany, 2019.
[62] N.A. Usov, Iron oxide nanoparticles for magnetic hyperthermia, Spin 9 (2) (2019) 1940001, https://doi.org/10.1142/S2010324719400010.
[63] N.A. Usov, E.M. Gubanova, Z.H. Wei, Specific absorption rate of assembly of magnetic nanoparticles with uniaxial anisotropy, J. Phys. Conf. 1439 (1) (2020) 012044, https://doi.org/10.1088/1742-6596/1439/1/012044.
[64] N.A. Usov, R.A. Rytov, V.A. Bautin, Properties of assembly of superparamagnetic nanoparticles in viscous liquid, Sci. Rep. 11 (1) (2021) 6999. https://www.nature.com/articles/s41598-021-86323-x.
[65] J.O. Andersson, C. Djurberg, T. Jonsson, P. Svedlindh, P. Nordblad, Monte Carlo studies of the dynamics of an interacting monodispersive magnetic-particle system, Phys. Rev. B 56 (1997) 13983. https://link.aps.org/doi/10.1103/PhysRevB.56.13983.
[66] É. Martin, Y. Gossuin, S. Bals, S. Kavak, Q.L. Vuong, Monte Carlo simulations of the magnetic behaviour of iron oxide nanoparticle ensembles: taking size dispersion, particle anisotropy, and dipolar interactions into account, Eur. Phys. J. B 95 (2022) 201, https://doi.org/10.1140/epjb/s10051-022-00468-w.
[67] A. Satoh, M. Aoshima, 3D Monte Carlo simulations of a magnetic disk-like particle dispersion, Colloid Polym. Sci. 289 (2011) 53–62, https://doi.org/10.1007/s00396-010-2320-9.
[68] H. Mamiya, H. Fukumoto, J.L.C. Huaman, K. Suzuki, Estimation of magnetic anisotropy of individual magnetite nanoparticles for magnetic hyperthermia, ACS Nano 14 (7) (2020) 8421–8432, https://doi.org/10.1021/acsnano.0c02521.
[69] R.E. Rosensweig, Heating magnetic fluid with alternating magnetic field, J. Magn. Magn Mater. 252 (2002) 370–374, https://doi.org/10.1016/S0304-8853(02)00706-0.
[70] S. Ruta, R. Chantrell, O. Hovorka, Unified model of hyperthermia via hysteresis heating in systems of interacting magnetic nanoparticles, Sci. Rep. 5 (2015) 9090, https://doi.org/10.1038/srep09090.